



# 11.00

## White Paper on Channel Modeling and Simulation for Reconfigurable Intelligent Surface

# Contributors

Organizations	Contributors
Beijing University of Posts and Telecommunications	Zhang Jianhua ( <a href="mailto:jhzhang@bupt.edu.cn">jhzhang@bupt.edu.cn</a> ) Zhang Yuxiang ( <a href="mailto:zhangyx@bupt.edu.cn">zhangyx@bupt.edu.cn</a> ) Gong Huiwen ( <a href="mailto:birdsplan@bupt.edu.cn">birdsplan@bupt.edu.cn</a> ) Zhang Jiwei ( <a href="mailto:rediaose@bupt.edu.cn">rediaose@bupt.edu.cn</a> ) Zhang Shiyu ( <a href="mailto:zhangsy@bupt.edu.cn">zhangsy@bupt.edu.cn</a> )
Southeast University	Cui Tiejun ( <a href="mailto:tjcui@seu.edu.cn">tjcui@seu.edu.cn</a> ) Jin Shi ( <a href="mailto:jinshi@seu.edu.cn">jinshi@seu.edu.cn</a> ) Cheng Qiang ( <a href="mailto:qiangcheng@seu.edu.cn">qiangcheng@seu.edu.cn</a> ) Li Xiao ( <a href="mailto:li_xiao@seu.edu.cn">li_xiao@seu.edu.cn</a> ) Sang Jian ( <a href="mailto:sangjian@seu.edu.cn">sangjian@seu.edu.cn</a> ) Tang Wankai ( <a href="mailto:tangwk@seu.edu.cn">tangwk@seu.edu.cn</a> )
Beijing Jiaotong University	He Ruisi ( <a href="mailto:ruisi.he@bjtu.edu.cn">ruisi.he@bjtu.edu.cn</a> ) Ai Bo ( <a href="mailto:boai@bjtu.edu.cn">boai@bjtu.edu.cn</a> ) Yuan Yuan ( <a href="mailto:22110033@bjtu.edu.cn">22110033@bjtu.edu.cn</a> )
ZTE Corporation	Dou Jianwu ( <a href="mailto:dou.jianwu@zte.com.cn">dou.jianwu@zte.com.cn</a> ) Zhao Yajun ( <a href="mailto:zhao.yajun1@zte.com.cn">zhao.yajun1@zte.com.cn</a> ) Jian Mengnan ( <a href="mailto:jian.mengnan@zte.com.cn">jian.mengnan@zte.com.cn</a> )
Huawei Technologies Co., Ltd.	Liu Yong ( <a href="mailto:liu.liuyong@huawei.com">liu.liuyong@huawei.com</a> )
China Mobile	Yuan Yifei ( <a href="mailto:yuanyifei@chinamobile.com">yuanyifei@chinamobile.com</a> ) Su Xin ( <a href="mailto:suxin@chinamobile.com">suxin@chinamobile.com</a> )
China Telecom	Cheng Zhenqiao ( <a href="mailto:chengzq@chinatelecom.cn">chengzq@chinatelecom.cn</a> ) Li Nanxi ( <a href="mailto:linanxi@chinatelecom.cn">linanxi@chinatelecom.cn</a> )
China Unicom	Liu Qiuyan ( <a href="mailto:liuqy95@chinaunicom.cn">liuqy95@chinaunicom.cn</a> ) Zhao Mingyang ( <a href="mailto:zhaomy65@chinaunicom.cn">zhaomy65@chinaunicom.cn</a> )

**Citation:** T. J. Cui, J. H. Zhang, J. W. Dou, S. Jin, Y. F. Yuan, Q. Y. Liu, N. X. Li et al. “Channel Modeling and Simulation for Reconfigurable Intelligent Surface,” FuTURE Forum, Nanjing, China, Apr 2025, doi: 10.12142/FuTURE.202504004.

## Preface

The rapid advancement of wireless communication technologies has led to an increasing demand for more efficient and intelligent communication systems. Reconfigurable Intelligent Surfaces (RIS) have emerged as a promising solution to address the challenges of future wireless networks, such as high spectral efficiency, low latency, and enhanced coverage. RIS, based on configurable metamaterials, can manipulate the propagation of electromagnetic waves by adjusting the phase or amplitude of wireless signals, thereby creating programmable wireless environments. This technology has the potential to revolutionize the way we design and optimize communication systems.

Accurate channel modeling and simulation are crucial for evaluating the performance of RIS in various scenarios and for guiding the development of RIS-related technologies. As one of the key technologies for future 6G networks, significant efforts have been made to develop channel models that can capture the unique characteristics of RIS-assisted communication links. This white paper aims to provide a comprehensive overview of the channel modeling and simulation work for RIS, highlighting the latest research findings and offering insights for future research directions. By presenting detailed channel models, system-level simulation results, and discussions on key technical issues, this paper seeks to contribute to the ongoing standardization efforts and promote the development and application of RIS technologies in future wireless communication systems.

# Contents

1.	Introduction .....	5
2.	Channel Model.....	7
2.1.	General Framework.....	7
2.2.	RIS Physical Model.....	9
2.3.	Path Loss Model.....	12
2.4.	Fast Fading Model.....	14
2.5.	Model Complexity Reduction .....	16
2.6.	New Features.....	17
3.	System-Level Simulation .....	18
3.1.	Simulation Case 1 .....	18
3.1.1.	System Assumptions .....	18
3.1.2.	Simulation Results .....	22
3.2.	Simulation Case 2 .....	27
3.2.1.	Simulation Assumptions .....	27
3.2.2.	Simulation Results .....	30
4.	Conclusion.....	33
	Acronyms .....	35
	Reference.....	37

# 1. Introduction

Reconfigurable Intelligent Surface (RIS) has the potential capability to build low-cost and low-power communication environments. Based on configurable metamaterials, RIS controls the propagation direction of electromagnetic waves by adjusting the phase or/and amplitude of wireless signals to build programmable wireless propagation environments. As an emerging technology, RIS cannot be evaluated and optimized without accurate channel models. Channel modeling and simulation can evaluate the performance of RIS in different frequency bands (e.g., below 6 GHz and millimeter-wave bands), optimize the design of RIS units, control algorithms, and beamforming strategies to improve the performance of the communication system, and provide an important technological foundation and data support for RIS-related research to promote 6G standardization.

3GPP Release 19 is an important version of 5G Advanced, which aims to further improve the performance of 5G systems and lay the foundation for 6G technologies. The channel modeling work in Release 19 focuses on the requirements of potential technologies for 6G. **The RIS channel modeling work starts from the channel model of 3GPP TR 38.901 (5G) and evolves and enhances based on the channel modeling work of Release 19.**

- **Integrated sensing and communication (ISAC) channel modeling:** the ISAC channel modeling study in Release 19 will provide the basis for the convergence of communication and environmental sensing. This is consistent with the goals of RIS technology, which can reconfigure the wireless environment by tuning reflections to optimize communication and sensing performance.
- **7~24 GHz band channel model validation:** Release 19 will validate the channel model within the 7-24 GHz band, which provides data support for the application of RIS in higher frequency bands. The optimization of the performance of RIS technology in higher frequency bands requires accurate channel models to guide it, especially when the size of the RIS panels is large, which produces significant near field effects and belongs to the current stage of the 3GPP RAN WG1 channel modeling research scope.

So far, 6 meetings of 3GPP RAN WG1 #116, #116bis, #117, #118, #118bis, and

#119 have been held in the 3GPP Release 19 phase, and a total of 43 agreements related to ISAC channel modeling have been concluded, as shown in Table 1-1. In excluding the aspects of ISAC-specific channel modeling, there are five categories of topics that involve solutions that can be borrowed for the RIS channel modeling standardization process:

- Target channel modeling: RIS cascade channel modeling.
- Target modeling: RIS physical modeling.
- Model simplification: RIS cascade channel model simplification.
- Target channel coupling to background channel: RIS cascade channel coupling to BS-UE channel.
- New features of the model.

This white paper will also discuss the content of channel modeling from the above five aspects.

**Table 1-1 Comparison of topics discussed in the 3GPP ISAC standardization with RIS**

ISAC-Channel Modeling		RIS-Channel Modeling	
Topics	Discussion	Key points	Sections
<b>Target channel modeling</b>	Whether the target channel is cascaded convolution or single point	<b>RIS cascade channel modeling</b>	2.1, 2.3 and 2.4
<b>Target modeling</b>	Target modeling based on the RCS scheme RCS is categorized into large and small scales	<b>RIS Physical Model</b>	2.2
<b>Model simplification</b>	Simplified schemes for cluster or path deleting, and multipath matching	<b>RIS Cascade channel simplification</b>	2.5
<b>Coupling of target channel and background channel</b>	The target channel and the background channel need to be power normalized	<b>RIS Cascaded channel coupled to BS-UE channel</b>	2.3

<b>New features</b>	Spatial consistency	<b>New features</b>	2.6
<b>ISAC-specific features</b>	Monostatic modeling, environment object modeling, target micro-Doppler, blockage modeling, typical target RCS classification modeling, RCS randomness	\	\

## 2. Channel Model

### 2.1. General Framework

The channel modeling framework for RIS-assisted communication links differs from the traditional communication modeling framework. As illustrated in Figure 2-1, conventional communication channels focus exclusively on the link between the transmitter (BS) and receiver (UE). In contrast, the channel modeling of RIS-assisted communication requires consideration of three interconnected components: the BS-RIS channel, the RIS-UE channel, and the physical model of the RIS itself.

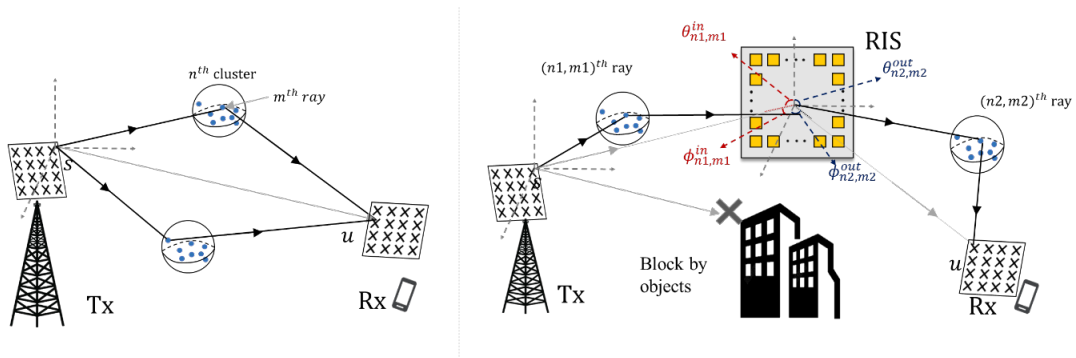


**Figure 2-1 Comparison Between Traditional Communication Models and RIS-Assisted Communication Channel Models**

Therefore, compared to traditional communication channels, the core of RIS channel modeling lies in accurately capturing channel characteristics in the propagation environment through high-precision yet low-complexity modeling methods, while

enabling channel simulation across a wide range of frequencies, bandwidths, and various application scenarios. To achieve this, RIS channel modeling must meet the following requirements:

- First, high-precision link modeling requires independent modeling of the BS-RIS and RIS-UE links, while considering the interrelationship between multiple links to accurately reflect path loss and scattering characteristics in the channel.
- Second, high-precision phase shift modeling of the RIS needs to account for its scattering pattern, ideal phase shifts, and angle dependencies, while also incorporating the non-ideal quantization effects present in real environments.
- Moreover, the model should be capable of simulating complex scenarios, including UMi, UMa, InH, and IIoT, allowing flexible adjustments for the locations of base stations, user terminals, and the RIS.

To achieve accurate simulation at the link level, the RIS channel model must handle multipath fading, reflecting channel fading characteristics in complex environments. Additionally, physical simplifications and optimizations of system simulations are necessary to improve modeling efficiency.

The framework of RIS channel modeling is addressed with considerations in the following proposals.

#### **Proposal 1: The assumption for the framework of RIS channel modeling and enhancement of 3GPP TR 38.901 [1]:**

- 1) The methodology in 3GPP TR38.901 is the start point of RIS channel modeling.

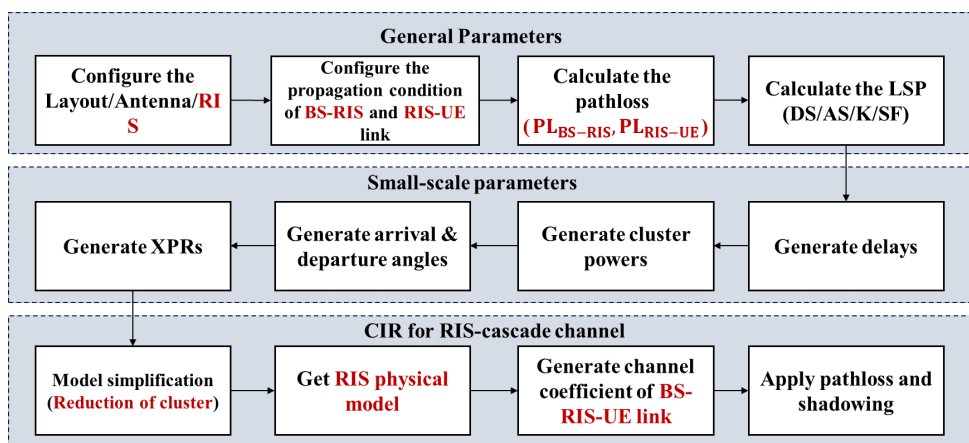


**Figure 2-2 RIS channel model implement based on the start point of 3GPP TR 38.901**

- 2) The per-hop basic channel model between BS-UE, BS-RIS, RIS-RIS or RIS-UE are constructed based on the enhanced 3GPP TR38.901 channel model, where the isotropic antenna is assumed for basic channel model.
- 3) A physical RIS panel with the pre-defined phase-shift code book for RIS elements can be represented by virtual RIS base stations induced by impinging EM waves with different delays, incident or polarization.
- 4) What are expected to be enhanced in 3GPP TR38.901 include:
  - Height dependent PL/LOS probability model.
  - Absolute time of arrival model.
- 5) The final channel model between BS and UE are comprehensive of direct path and cascaded path:
  - Direct path: BS-UE channel.
  - Cascaded path: BS-RIS-UE channel.

## 2.2. RIS Physical Model

The physical model of a RIS is fundamentally based on defining the radiation pattern of RIS array elements, also known as Radar Cross Section (RCS). Currently, the main methods for modeling RIS include the following:

**Physical model based on equivalent radiation pattern [2]:** This model represents the RIS response to signals through an equivalent radiation pattern. It first derives the field distribution of RIS elements using physical optics, then applies the equivalence principle to calculate the secondary radiation of the elements. The radiation pattern of each RIS element is defined and computed, ultimately forming the overall radiation pattern of the RIS.

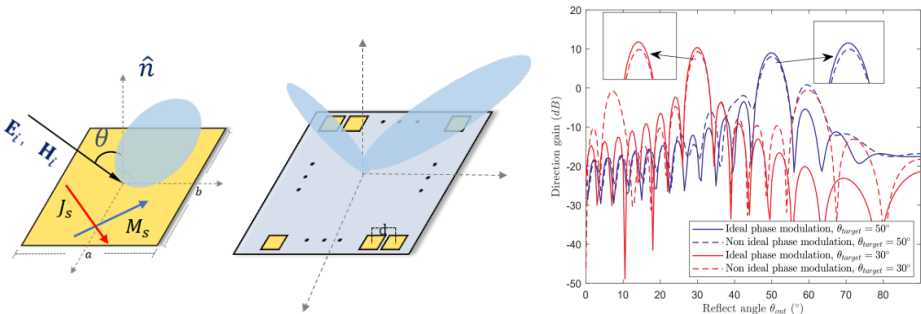
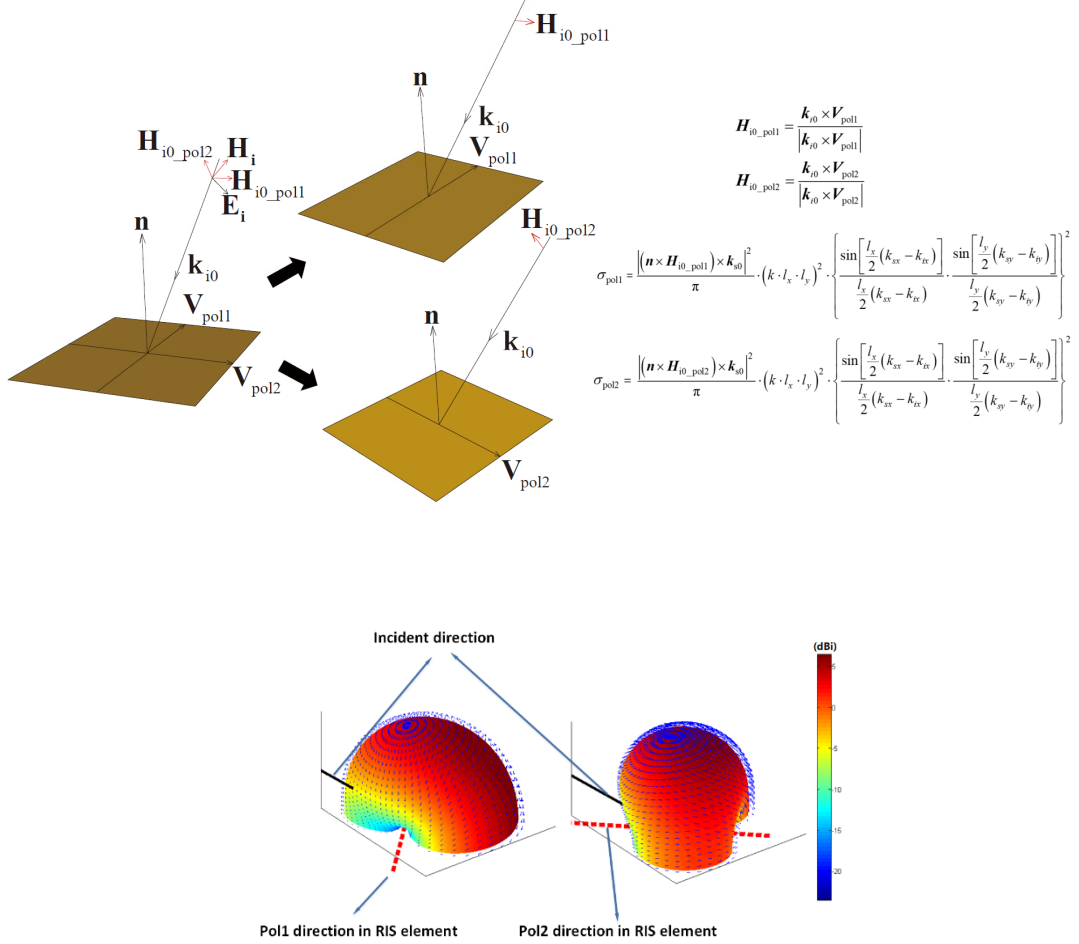


Figure 2-3 The illustration of RIS equivalent radiation pattern [2]

**RCS Model Based on Electromagnetic Theory [3][21]:** This method uses electromagnetic theory to establish accurate RCS models under different polarization

conditions. This modeling approach accurately describes the reflection characteristics of RIS elements in complex electromagnetic environments, providing a theoretical foundation for evaluating the performance of RIS.



**Figure 2-4 RCS-based polarized RIS element pattern[21]**

**Simplified Cosine Radiation Pattern Model [4]:** This model uses a simplified antenna radiation pattern assumption and adopts the  $\cos^\alpha \theta$  model to describe the directional characteristics of RIS elements. While this method is computationally simple and suitable for scenarios with lower system requirements, its accuracy may be inferior to that of the RCS model based on electromagnetic theory.

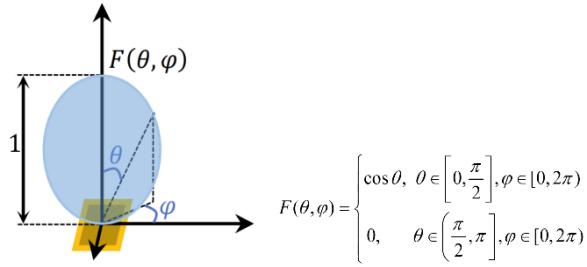


**Figure 2-5 Normalized power radiation pattern based on  $\cos^\alpha \theta$**

**Single Antenna Element Model in 3GPP TR 38.901[1]:** The radiated power pattern of a single antenna element, defined in 3GPP TR 38.901, is a model calculated based on specific formulas to characterize the radiation of an antenna in horizontal and vertical directions. Compared with the cosine model, the model in TR 38.901 is more complex and accurate, considering more parameters (e.g., 3 dB-beamwidth, sidelobe attenuation, etc.).

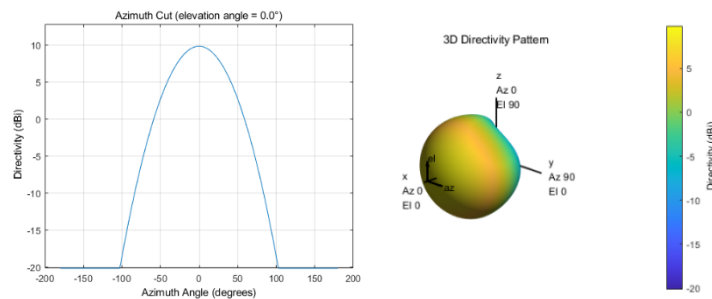


**Figure 2-6 Radiation power pattern of a single antenna element in 3GPP TR 38.901**

By comparing the differences between different physical models, the parameters of the simple model (e.g. the model in TR 38.901) are modified to achieve efficient and usable physical modeling. As shown in the figure, the differences in the equivalent radiation direction maps of the RIS obtained by the two types of methods, “physical optics” method-based model and “38.901” antenna model.

When the incoming wave is perpendicular to the RIS panel (coinciding with the normal) and the array element gain of the RIS is set to 5 dBi in the TR 38.901 method, the patterns of the two types of models are nearly the same; when the incoming wave is skewed, the two types of models will have some differences.

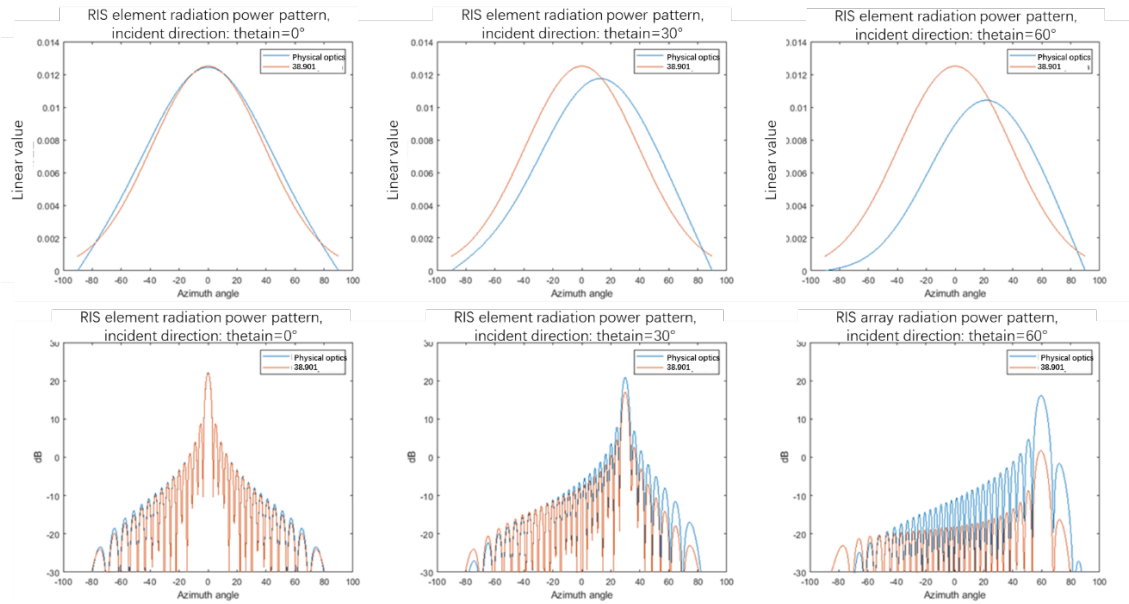


**Figure 2-7 Comparison of modeling schemes based on the physical optics method and those based on the 38.901 antenna model**

**Proposal 2: A more accurate physical optics-based RIS cell model can be approximated by parameter corrections based on the antenna element model in TR 38.901.**

### 2.3. Path Loss Model

The RIS path loss model can refer to the cascaded path loss modeling approach used in ISAC systems for target channels, where the BS-RIS-UE path loss is modeled as the combination of sub-channel path loss [8], RIS average radiation gain (or average RCS), and omnidirectional antenna aperture:

$$PL_{RIS}(d_1, d_2) = PL_{BS-RIS}(d_1) + PL_{RIS-UE}(d_2) + 10\log_{10}\left(\frac{\lambda^2}{4\pi}\right) - 10\log_{10}(\sigma_{RIS}). \quad (3-1)$$

where  $d_1, d_2$  refer to the distance from BS to RIS and the distance from RIS to UE.

Alternatively, the following modified floating-intercept (FI) and close-in (CI) path loss models can be considered:

Let  $\theta_i, \theta_r$  refer to the elevation angle-of-arrival (EAoA) from BS to RIS, and the elevation angle-of-departure (EAoD) from RIS to UE, respectively. Then, the path-loss

(PL) model for RIS-assisted cascaded channel is formulated as follows [9]:

**The modified floating intercept (FI) PL model** is written as

$$PL_{FI}^{RIS}(d_1, d_2, \theta_t, \theta_r) = \alpha + 10\beta_1 \log_{10}(d_1) + 10\beta_2 \log_{10}(d_2) - 10\lambda_1 \log_{10}(\cos(\theta_t)) - 10\lambda_2 \log_{10}(\cos(\theta_r)) + X_{\sigma}^{FI}, \quad (3-2)$$

where  $\beta_1$  and  $\beta_2$  are the path-loss exponents (PLEs) on  $d_1$  and  $d_2$ ;  $\lambda_1$  and  $\lambda_2$  are the PLEs on  $\theta_t$  and  $\theta_r$ ;  $\alpha$  denotes the intercept parameter of PL;  $X_{\sigma}^{FI}$  denotes the shadow factor (SF), which is modelled as Gaussian distribution.

**The modified close-in (CI) PL model** for RIS-assisted communications is

$$PL_{CI}^{RIS}(d_1, d_2, \theta_t, \theta_r) = PL_{FS}^{RIS}(d_0^1, d_0^2, \theta_0^t, \theta_0^r) + 10n_1 \log_{10}\left(\frac{d_1}{d_0^1}\right) + 10n_2 \log_{10}\left(\frac{d_2}{d_0^2}\right) - 10\mu_1 \log_{10}\left(\frac{\cos(\theta_t)}{\cos(\theta_0^t)}\right) - 10\mu_2 \log_{10}\left(\frac{\cos(\theta_r)}{\cos(\theta_0^r)}\right) + X_{\sigma}^{CI}, \quad (3-3)$$

where  $n_1$  and  $n_2$  are the PLEs on  $d_1$  and  $d_2$ ;  $\mu_1$  and  $\mu_2$  are the PLEs on  $\theta_t$  and  $\theta_r$ ;  $X_{\sigma}^{CI}$  is the SF following Gaussian distribution;  $d_0^1$ ,  $d_0^2$ ,  $\theta_0^t$ , and  $\theta_0^r$  denote the reference distances of  $d_1$  and  $d_2$  as well as the reference angles of  $\theta_t$  and  $\theta_r$ , respectively. These reference values can be adjusted appropriately in different scenarios where applicable.  $PL_{FS}^{RIS}(d_0^1, d_0^2, \theta_0^t, \theta_0^r)$  represents the PL under these reference variables in free space. It should be noted that the effects of the physical size, number of unit cells, reflection magnitude, reflection phase of RIS on the PL, have been integrated into the terms of  $PL_{FS}^{RIS}(d_0^1, d_0^2, \theta_0^t, \theta_0^r)$  and  $\alpha$  in the modified CI and FI models, respectively.

**Proposal 3: The empirical FI and CI models with low complexity, high accuracy and wide applicability are proposed to describe the path loss of RIS-assisted wireless communications.**

When coupling a cascaded channel with a direct channel, a power control factor needs to be added with the following expression

$$PL_{\text{cou}} = PL_{\text{cas}} + PL_{\text{dir}}$$

$$PL_{\text{dir}} = O_{\text{RIS}} \cdot PL_{\text{env}} \quad (3-4)$$

Where  $PL_{\text{cou}}$ : Overall channel path loss,  $PL_{\text{cas}}$ : Tx-RIS-Rx cascade channel path loss,  $PL_{\text{dir}}$ : Tx-Rx direct channel path loss,  $PL_{\text{env}}$ : Background channel path loss without RIS which can reuse the model in TR 38.901 and the measured  $O_{\text{RIS}}$  is obtained to be a random value following a normal distribution and subject to target correlation with the LOS states of Tx and Rx.

**Proposal 4: BS-RIS-UE cascaded channel coupled to BS-UE direct channel with the introduction of a new parameter Power Control Factor (PCF) modeling cascaded channel on direct channel loss.**

## 2.4. Fast Fading Model

Based on the GBSM model principle, the fast-fading model for the BS-RIS-UE link can be derived by extending the communication channel model from 3GPP TR 38.901. Using as the fundamental framework, if the BS has S transmitting antennas and the UE has U receiving antennas, the channel response coefficient from the s-th antenna at the BS to the u-th antenna at the UE through the RIS can be expressed as [2]:

$$h_{u,s}^{ris}(t, \tau) = \sum_{n_1, m_1}^{N_1, M_1} \sum_{n_2, m_2}^{N_2, M_2} \sqrt{P_{n_1, m_1} P_{n_2, m_2}} \begin{bmatrix} F_{rx,u}^v(\theta_{n_2, m_2}^{rx}, \phi_{n_2, m_2}^{rx}) \\ F_{rx,u}^h(\theta_{n_2, m_2}^{rx}, \phi_{n_2, m_2}^{rx}) \end{bmatrix}^T \cdot \begin{bmatrix} \exp(j\Phi_{n_2, m_2}^{vv}) & \sqrt{\kappa_{n_2, m_2}^{-1}} \exp(j\Phi_{n_2, m_2}^{vh}) \\ \sqrt{\kappa_{n_2, m_2}^{-1}} \exp(j\Phi_{n_2, m_2}^{hv}) & \exp(j\Phi_{n_2, m_2}^{hh}) \end{bmatrix} \\ \cdot \begin{bmatrix} F_{ris}^{vv}(\phi_{n_1, m_1}^{in}, \theta_{n_1, m_1}^{in}, \phi_{n_2, m_2}^{out}, \theta_{n_2, m_2}^{out}) & F_{ris}^{vh}(\phi_{n_1, m_1}^{in}, \theta_{n_1, m_1}^{in}, \phi_{n_2, m_2}^{out}, \theta_{n_2, m_2}^{out}) \\ F_{ris}^{hv}(\phi_{n_1, m_1}^{in}, \theta_{n_1, m_1}^{in}, \phi_{n_2, m_2}^{out}, \theta_{n_2, m_2}^{out}) & F_{ris}^{hh}(\phi_{n_1, m_1}^{in}, \theta_{n_1, m_1}^{in}, \phi_{n_2, m_2}^{out}, \theta_{n_2, m_2}^{out}) \end{bmatrix} \\ \cdot \begin{bmatrix} \exp(j\Phi_{n_1, m_1}^{vv}) & \sqrt{\kappa_{n_1, m_1}^{-1}} \exp(j\Phi_{n_1, m_1}^{vh}) \\ \sqrt{\kappa_{n_1, m_1}^{-1}} \exp(j\Phi_{n_1, m_1}^{hv}) & \exp(j\Phi_{n_1, m_1}^{hh}) \end{bmatrix} \cdot \begin{bmatrix} F_{tx,s}^v(\theta_{n_1, m_1}^{tx}, \phi_{n_1, m_1}^{tx}) \\ F_{tx,s}^h(\theta_{n_1, m_1}^{tx}, \phi_{n_1, m_1}^{tx}) \end{bmatrix} \\ \cdot \exp\left(j\frac{2\pi}{\lambda}(\mathbf{r}_{n_2, m_2}^{rx} \cdot \mathbf{d}_u^{rx} + \mathbf{r}_{n_1, m_1}^{tx} \cdot \mathbf{d}_s^{tx})\right) \cdot \exp(j2\pi f_{n_2, m_2} t) \cdot \delta(\tau - \tau_{n_1, m_1} - \tau_{n_2, m_2}). \quad (3-5)$$

- $(\cdot)^T$  stands for matrix transposition.
- $\lambda$  is the wavelength of the carrier frequency.

- $n_i, m_i$ ,  $i \in \{1, 2\}$  indicate the identifier of cluster and path in BS-RIS and RIS-UE sub-channels.
- and  $P_{n_2, m_2}$  are the power of the corresponding path.
- $\phi_{n_1, m_1}^{in}, \theta_{n_1, m_1}^{in}, \theta_{n_1, m_1}^{tx}, \phi_{n_1, m_1}^{tx}$  denote the angle of  $(n_1, m_1)^{th}$  path in BS-RIS sub-channel, which are the azimuth angle of arrival (AoA), the zenith angle of arrival (ZoA), the azimuth angle of departure (AoD), and the zenith angle of departure (ZoD) respectively. Similarly,  $\phi_{n_2, m_2}^{rx}, \theta_{n_2, m_2}^{rx}, \theta_{n_2, m_2}^{out}, \phi_{n_2, m_2}^{out}$  are the AoA, ZoA, AoD, ZoD of the  $(n_2, m_2)^{th}$  path in RIS-UE sub-channel.
- $\mathbf{r}_{n_2, m_2}^{rx}$  and  $\mathbf{r}_{n_1, m_1}^{tx}$  are the unit direction vector of corresponding path at receiver and transmitter. Additionally,  $\mathbf{d}_u^{rx}$  and  $\mathbf{d}_s^{tx}$  indicate the location vectors of antenna  $u$  and  $s$ .
- $p_1, p_2 \in \{v, h\}$  denote the vertical and horizontal polarization direction.
- $F_{rx, u}^v, F_{rx, u}^h, F_{tx, s}^v$  and  $F_{tx, s}^h$  indicate the radiation pattern of antenna  $u$  at UE and  $s$  at BS, in the  $v$  and  $h$  polarization, respectively.
- $F_{ris}^{p_1 p_2}$  denotes the radiation pattern of entire RIS.  $p_1 p_2$  indicates that RIS has different effects on the cluster or path incident in the  $p_1$  polarization direction and emitted in the  $p_2$  polarization direction. The generation method of this radiation pattern can refer to the three methods in Chapter 3.2.
- $\Phi_{n_i, m_i}^{p_1 p_2}$ ,  $i \in \{1, 2\}$  is the random phase of the  $(n_i, m_i)^{th}$  path that depart with  $p_1$  polarization and arrive with  $p_2$  polarization.  $\kappa_{n_i, m_i}$ ,  $i \in \{1, 2\}$  is the cross-polarization power ratio (XPR) of the corresponding path.
- $f_{n_2, m_2}$  is the Doppler shift of the  $(n_2, m_2)^{th}$  path.
- $\tau_{n_i, m_i}$ ,  $i \in \{1, 2\}$  denotes the delay of the corresponding path.

The parameter generation method for the formula refers to Section 7.5 'Fast Fading' in 38.901[1]. It can be observed that the key to this small-scale model lies in matching the multipaths of the BS-RIS and RIS-UE two sub-channels one-to-one, which embodies the concept of convolution. Experimental validation of this model can be found in reference [10].

**Proposal 5:** The fast-fading component of the RIS channel needs to account for the cascading effect of the BS-RIS link, the RIS radiation pattern, and the RIS-UE link. A cascaded channel model based on GBSM can be considered, with model parameters generated according to 3GPP TR 38.901.

## 2.5. Model Complexity Reduction

All fast-fading models proposed in Section 3.3.2 are based on the BS-RIS-UE link, which is derived from the cascading of the BS-RIS and RIS-UE subchannels. Although the convolutional cascading method can accurately describe the channel model of this link, it poses the challenge of high model complexity: If the full convolution is performed at the ray level, where the BS-RIS channel contains  $N_1 \cdot M_1$  rays and the RIS-UE channel contains  $N_2 \cdot M_2$  rays, then the resulting target channel will require  $N_1 \cdot M_1 \cdot N_2 \cdot M_2$  computations, which might lead to an unacceptable simulation time cost. Therefore, it is necessary to explore ways to reduce the complexity of concatenation channels.

Considering the following potential simplification methods:

**Table 2-1 Potential simplification methods**

<b>Classifications</b>	Drop clusters based on power (proportion/threshold)	
<b>Order</b>	Drop before convolution	Drop while convolution
<b>Method</b>	Method 1 Based on power ratio	Method 2 Based on 25 dB threshold
<b>Expected effect</b>	$N_{m1} M_1 N_{m1} M_2$	$N_{m2} M_1 N_{m2} M_2$

These methods can be considered for implementation in Step 9 *Model simplification (Reduction of cluster)* of **Figure 2-2**

It is recommended to consider Method 1 and Method 2 because they efficiently compute while effectively retaining the main characteristics of the channel. Method 1 prioritizes high-power clusters to ensure important paths remain intact, while Method 2 uses power thresholds to control complexity and simplify the signal. Both methods

achieve a good balance between performance and computational burden, making them suitable for large-scale simulations.

**Proposal 6: The following multipath convolution simplification methods can be considered:**

- Option 1: Retain the clusters with the highest power proportions in subchannels and convolve the remaining ones at the ray level.
- Option 2: Arrange the subchannel clusters in descending order of power, set a 25 dB power threshold, and prune during convolution.

## 2.6. New Features

**Parameters update:** Considering the actual deployment scenarios of RIS, base stations, terminals, or other elements may differ from the existing configuration in TR 38.901, the following parameters need to be considered for updates.

**Table 2-2 RIS-related parameters update**

Parameter	Description
<b>Path-loss exponents (PLEs)</b>	Path loss model parameters that may need adjustment.
<b>LOS probability</b>	Update the LOS for both RIS and UE.
<b>Rician K-factor</b>	Represents the ratio of direct to scattered signal power.
<b>Delay Spread (DS) [12]</b>	Represents the signal delay variations over time.
<b>Spread of Angle (ASA/ASD/ZSA/ZSD)</b>	Measures the angular spread of sub-channels.
<b>Others</b>	Other parameters that may require consideration.

**Near-field propagation:** Due to the passive and low-cost nature of RIS, it can be made large. According to the near-field distance formula, both BS and UE are likely to fall within the near-field range of the RIS panel, necessitating the consideration of near-

field propagation characteristics [4][13]-[17].

**Spatial consistency:** RIS can be used to ensure channel stability for moving objects, making it essential to characterize the spatial consistency of UE channels at different positions [13]-[17].

**The reciprocity of uplink and downlink:** The channel discrepancy between TDD and FDD systems assisted by RIS needs to be discussed [18].

## 3. System-Level Simulation

*The content of this chapter is intended as a point of reference, to serve as a foundation upon which a more optimal system simulation configuration can be developed.* To this end, it is essential to engage in further discourse with the academic and industrial communities to reach a consensus on a configuration that is both academically sound and aligned with industrial standards.

### 3.1. Simulation Case 1

#### 3.1.1. System Assumptions

##### 3.1.1.1. Simulation Parameters

The main parameters of the system level simulations are summarized in Table 3-1.

**Table 3-1 Simulation set up and parameters**

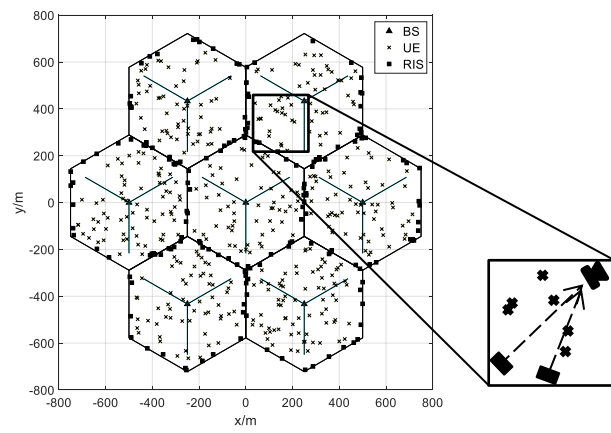
Parameter	Value
Number of cells	7 (e.g., 21 sectors), hexagonal macro
Operating band	2.6 GHz
Site-to-site dist.	500 m
Number of RIS panels per sector	4, 8, or 24, min distance of 25 m between RIS panels, uniformly distributed or at cell edges (e.g., 0.9~1.0 cell radius)

RIS antenna orientation	Facing towards its serving BS (azimuth)
Number of mobiles per sector	50 (100% outdoor), uniformly distributed or at cell edges (e.g., 0.85~0.9 cell radius)
BS antenna height	25 m
BS antenna down-tilt	0° (mechanical) and 4° (electronic)
RIS panel height	15 m
RIS panel down-tilt	10° (mechanical)
Mobile antenna height	1.5 m
BS transmit power	46 dBm
BS antenna gain	17 dBi for sector beam
Polarization	Vertical
MS antenna config	1×2, with random orientation
Pathloss model	ITU-Urban Macro for BS-RIS, RIS-UE and BS-UE links
RIS antenna pattern	BS antenna pattern in 3GPP TR 38.901, separately modeled for the cascaded link, total gain of 5 dBi at boresight
Number of elements per RIS panel	16×16, or 40×40, with 0.4λ spacing both vertically and horizontally
Number of bits for RIS element phase	2 bits
Combining of RIS cascaded link and direct link	Non-coherent, e.g., gains added up

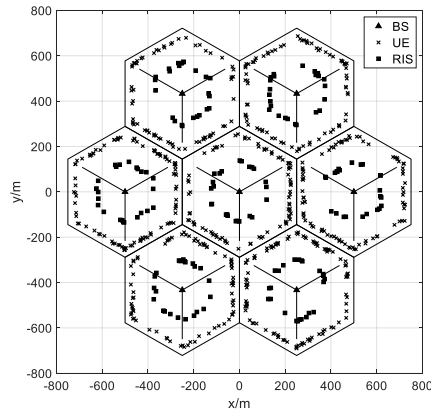
### 3.1.1.2. Network layout model

Figure 3-1 (a) shows the network layout of the system level simulation when RISs

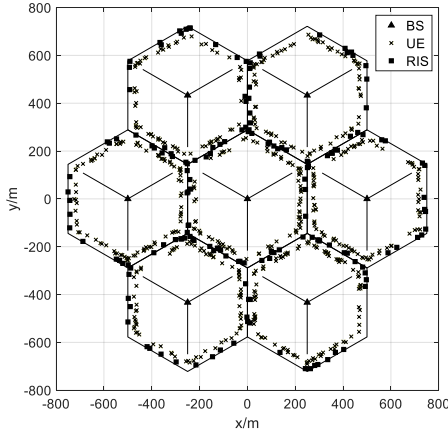
are at cell edges and mobiles are uniformly distributed over the entire network. The rectangular on the right is the partially enlarged figure of a cell. The normal directions of RIS panels are all facing toward the serving base stations of those cells. Figure 3-1 (b) is the system layout where RISs are placed around near the middle of cells, e.g., halfway from their serving base stations and halfway from the cell edges, and mobiles are placed at cell edges, with the partially enlarged figure on the right. It is seen that the normal directions of RIS panels are perpendicular to the normal directions of serving base station antennas. Figure 3-1 (c) shows the layout when both RIS panels and mobiles are at cell edges.[19]



(a) RIS at cell edges, mobiles uniformly distributed



(b) RIS in the middle of cells, mobiles at cell edges



(c) Both RIS and mobiles at cell edges

**Figure 3-1 Network layout with RIS and mobiles**

### 3.1.1.3. Inter-cell interference

As a type of passive device, RIS may reflect any signal it receives if the signal is within the passing band of the RIS device. Hence, potential interference should be considered in system level simulations that include multiple base stations, RIS panels and mobiles. This is crucial to ensure the comprehensiveness and the accuracy of the simulations. Figure 3-2 illustrates a scenario where there are two base stations, multiple RIS panels and a mobile. The interference received by the mobile not only comes directly from its neighboring base station, but also from neighboring base stations that are reflected by the RIS panels in the neighboring cells, as well as reflected by the nearest RIS panel in the serving cell. Note that the pathlosses from neighboring base station to RIS panels in the serving cell are usually severe. The pathlosses from RIS panels in the serving cell (except the nearest RIS panel) are also big. Hence, the interference from neighboring base station, reflected by RIS panels of the serving cell (except the nearest RIS panel) is ignored in the system level simulations.

No intra-cell interference is assumed, e.g., mobile users of the same cell would be allocated with orthogonal resources. Hence, the serving cell's signal reflected by non-serving RIS panels would not be the interference, rather considered to be the signal. However, since the element phases of non-serving RIS panels in general are not suitable for the mobile being studied and simulated, that part of the signal contribution is quite small and can often be ignored.

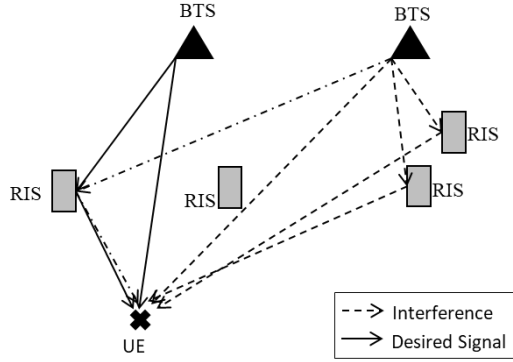


**Figure 3-2 Interference situation in scenario with two base stations and multiple RIS panels**

### 3.1.1.4. Beam forming methods: optimal phase

In the system level simulations, the angles of departures and angles of arrivals are known once the locations of base stations, RIS panels and mobiles are fixed. Also, BS-RIS channel is assumed LOS dominant. Hence, the optimal phase of the element in  $l$ -th row and  $k$ -th column of a RIS panel (ignoring interference) can be determined according to the incident angle and reflected angle:

$$\Phi_{l,k} = -2\pi \frac{(\hat{r}_{\text{ZOA RIS}, \text{AOA RIS}}^T + \hat{r}_{\text{ZOD RIS}, \text{AOD RIS}}^T) \bar{d}_{l,k}}{\lambda} \quad (3-1)$$

Here the index of RIS elements is two-dimensional, corresponding to the position of each element in the rectangular RIS panel. To more precisely capture the characteristics of metasurface devices in real deployment, 2-bit phase quantization is assumed for each element, with the following formula:

$$\Phi_{l,k} = \begin{cases} \frac{\pi}{4}, & 0 \leq \text{mod}(\Phi_{l,k}, 2\pi) < \frac{\pi}{2} \\ \frac{3\pi}{4}, & \frac{\pi}{2} \leq \text{mod}(\Phi_{l,k}, 2\pi) < \pi \\ -\frac{3\pi}{4}, & \pi \leq \text{mod}(\Phi_{l,k}, 2\pi) < \frac{3\pi}{2} \\ -\frac{\pi}{4}, & \frac{3\pi}{2} \leq \text{mod}(\Phi_{l,k}, 2\pi) < 2\pi \end{cases} \quad (3-2)$$

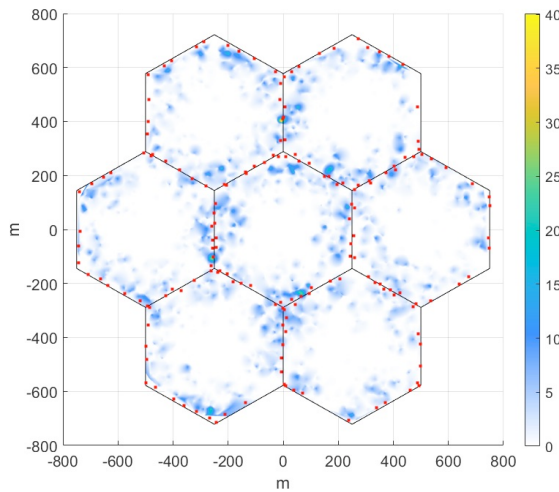
## 3.1.2. Simulation Results

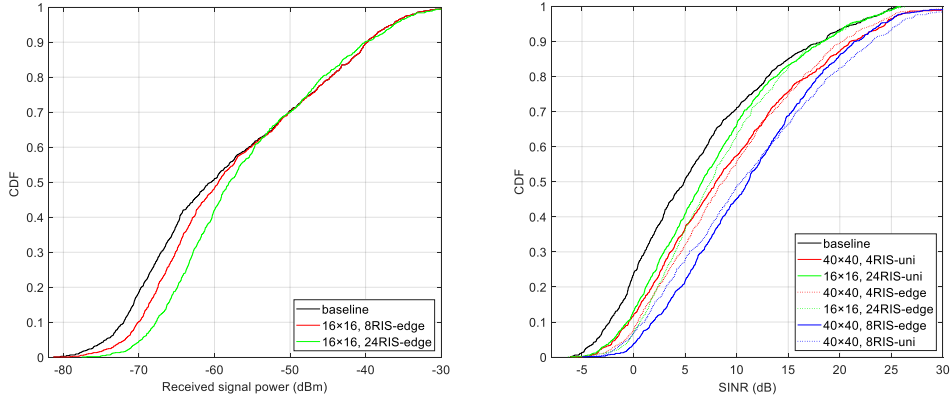
### 3.1.2.1. Impact of RIS deployments

Figure 3-3 shows the cumulative distribution functions (CDF) of the RSRP. The UE

and RIS panels are distributed near the cell edges, with the consideration that the RSRP is a coverage-oriented metric and that it is likely that the mobiles near the cell edges would have coverage issue in a 2.6 GHz deployment. When each RIS panel has  $16 \times 16$  elements, the beam-width of the main lobe is about  $7.4^\circ$  without special codebooks, which is wide enough to cover the area served by the RIS panel. A heat map illustrating the geo-distribution of the RSRP gains within the considered 7-cell (21-sector) network is provided, which shows the coverage area of each RIS panel as well. The red dots on the map denote the locations of the RIS panels. The small blue clusters represent areas where the deployment of RIS panels results in RSRP gains compared to the baseline system (without RIS)[20]

Figure 3-3 shows seven CDF curves of SINR, varying with the locations, number, and size of RIS panels. For 24 RIS panels of  $16 \times 16$  elements per sector (solid green for uniform distribution, dashed magenta for cell-edge) and 4 RIS panels of  $40 \times 40$  elements (solid red for uniform, dashed cyan for cell-edge), the total RIS elements per sector are nearly equal (6144 vs. 6400). Results indicate that deploying fewer, larger RIS panels ( $40 \times 40$ ) is preferable to deploying more, smaller panels ( $16 \times 16$ ) in both uniform and cell-edge deployments. SINR performance is similar for both strategies, though it spreads more widely with uniform distribution. Increasing the number of  $40 \times 40$  RIS panels per sector from 4 to 8 (solid blue for cell-edge, dashed blue for uniform) raises the average SINR gain from 4 dB to 7 dB.





**Figure 3-3 CDF of downlink RSRP and SINR for different RIS deployments**

### 3.1.2.2. Near field analysis

Figure 3-4 shows the CDFs of the distance between an RIS panel and the served UEs. The RIS panels are deployed either at the cell edges (solid blue line for  $16 \times 16$  RIS and solid red line for  $40 \times 40$  RIS) or uniformly distributed (dashed blue line for  $16 \times 16$  RIS and dashed red line for  $40 \times 40$  RIS). The UEs are uniformly distributed. The criterion utilized for the RIS-UE pairing is that the path gain of the BS-RIS-UE cascaded link is no less than 3 dB than the path gain of the BS-UE direct link. When  $16 \times 16$  element RIS panels are deployed, the aperture is 1.0 m. The corresponding Rayleigh distance is roughly 19 m (dashed black line), which is much shorter than the typical distance between a UE and its serving RIS panel as seen in Fig. 2. In other words, the propagation occurs predominantly in the far field. When  $40 \times 40$  element RIS panels are deployed, however, the aperture becomes 2.6 m. The corresponding Rayleigh distance is 118 m (dashed magenta line). According to Figure 3-4, there is roughly 50% of probability that a UE would be within 118 m from its serving RIS panel, i.e., the propagation occurs in the near field.

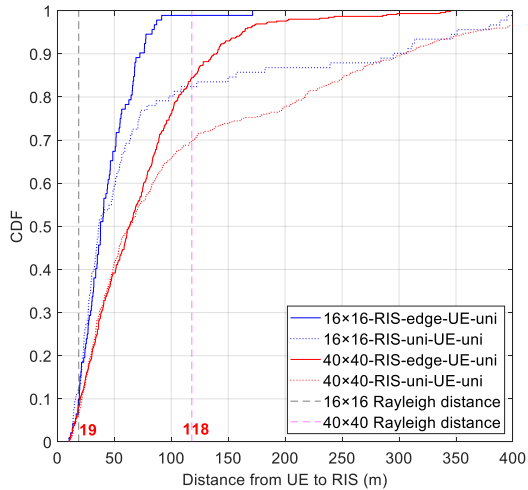


**Figure 3-4 CDFs of the distance between a RIS panel and its served UE**

### 3.1.2.3. Impact of interference modeling

As a nearly passive device, an RIS cannot differentiate between desired signals and interference. Consequently, it may reflect interference as if it were a desired signal, potentially degrading performance. In the downlink, a UE can experience interference not only from its neighboring BS but also from reflections of RIS panels in neighboring cells and its serving sector. Figure 3-5 compares the SINR distribution with and without considering cross-RIS interference. RIS panels are located at cell edges, and UEs are uniformly distributed across the network. The results show that the difference is not significant for either the 16×16 element RIS or the 40×40 element RIS. This can be explained as follows: For smaller RIS panels (e.g., 16×16 elements), the coverage area is limited (50% percentile at 37 m, per Figure 3-4), reducing the likelihood of a UE being within the coverage of a non-serving RIS panel. For larger RIS panels (e.g., 40×40 elements), although the coverage area increases (50% percentile at 59 m, per Figure 3-4), the narrow beamwidth ( $2.6^\circ$ ) minimizes the probability of cross-RIS interference. Thus, cross-RIS interference appears to have minimal impact on system-level performance.

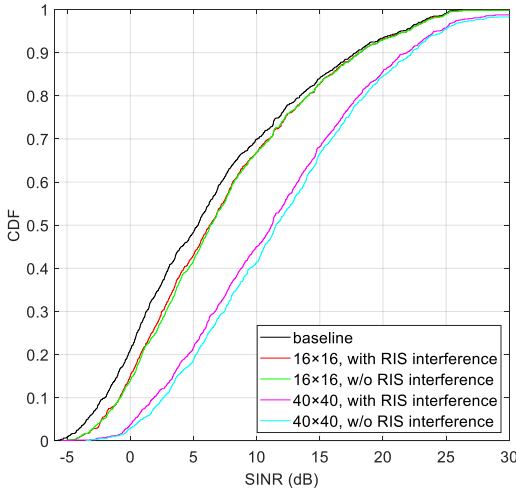


**Figure 3-5 CDF of the downlink SINR with and without (w/o) cross RIS interference modeling**

Some important insights can be drawn which may be useful for future studies and deployments of RIS.

The effectiveness of an RIS panel, a nearly passive device without power amplifiers, is fundamentally determined by its total aperture. Whether to deploy more smaller panels or fewer larger panels depends on factors such as network layout and channel model. In the typical 3GPP setting operating at 2.6 GHz, deploying fewer larger RIS panels is preferable. **This suggests focusing on designing larger panels rather than finding suitable deployment sites.** In future 6G mid-band applications (e.g., 6.7 GHz), a  $40 \times 40$  RIS panel with half-wavelength spacing has an area of approximately  $0.9 \times 0.9$  m $^2$ , which is manageable for realistic deployments. However, increasing panel size with fixed element spacing raises hardware costs due to additional diodes and more complex driving circuits. Using wider element spacing (e.g., greater than half a wavelength) can mitigate hardware complexity while still benefiting from aperture gain.

As RIS panel aperture increases, **near-field propagation dominates the RIS-UE link**, rendering far-field codebooks suboptimal. New codebook designs for RIS phase shifts, channel state information (CSI) estimation, and feedback are necessary.

**Interference from RIS panels may be less significant than initially thought.** To compensate for path loss in cascaded links, RIS panels form narrow beams toward desired directions. For larger panels, narrow beams are common, reducing the likelihood of interfering with other network nodes. This consideration applies to

coexistence scenarios with adjacent operating bands. Although RIS panels lack filters to confine signals within their operating band, the narrow beamwidths minimize the risk of involuntary interference to adjacent bands.

## 3.2. Simulation Case 2

### 3.2.1. Simulation Assumptions

#### 3.2.1.1. System-level simulation methodology

The system level simulation methodology should include the following key points.

##### ✧ Evaluation factors

The evaluation factors may include different specification parameter configurations such as the number of quantization bits, the number of RIS nodes, the number of RIS elements, and RIS locations, as well as typical phase configuration schemes such as beam sweeping-based scheme and channel estimation-based user-specific (UE-Specific) beamforming, and so on.

First, the array scale of the RIS reflector directly affects the array gain of the reflector. Observing and evaluating the trend of the UE SINR/throughput on RIS scales with practical networks assumptions is an effective method to evaluate the potential value of the RIS in the practical systems.

Second, the location or topology of the RIS nodes (as shown in Figure 3-6) can also greatly affect the actual performance of the RIS. The evaluation and verification of RIS panel height, panel orientation, panel tilt, azimuth, relative distance to other nodes is important for RIS performance measurement.

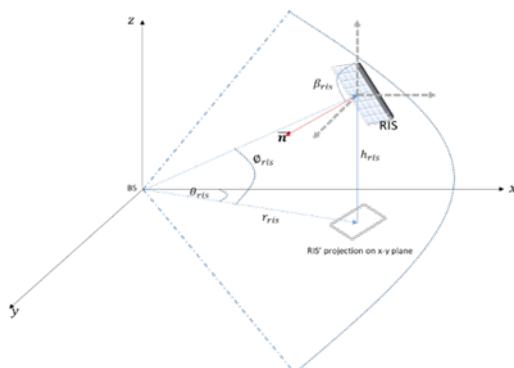


**Figure 3-6 Example of RIS location or topology**

Thirdly, considering the general assumption of passive characteristics of RIS, the relative distribution of BS, RIS, and UE is of great value to the definition of RIS beneficial scenarios. The impact of the distribution can be analyzed by introducing a parameter of beneficial UE ratio (BUR, Beneficial UE Ratio). Specifically, BUR metric may assess the number of potentially beneficial UEs associated with a particular RIS by comparing channel conditions (path loss, RSRP...) between cascaded channels and direct channels, which may be reflected by a particular channel condition threshold, for example, BUR can be defined as

$$BUR = \frac{NUM_A}{NUM_{All\_UE}}$$

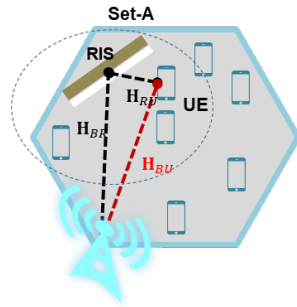


**Figure 3-7 Example of RIS BUR modeling**

Where set-A includes all the UEs satisfying the above threshold condition.

#### ❖ Evaluation metrics

The evaluation metrics at least include CDF of the SINR and RSRP, system throughput and CDF of user throughput.

On one hand, one of the RIS optimization objectives is to maximize the (direct and reflection) target signal power and minimize the interference power at the same time. Thus, UE SINR distribution is one of the most intuitive metrics that reflect RIS optimization effect.

On the other hand, the joint optimization of precoding on the BS and RIS sides can enhance the end-to-end equivalent channel of the BS-UE, which can be converted into an enhancement of the user-perceived rate. In practical performance evaluation, the UE throughput distribution curve can reflect the impact of the RIS on the throughput of different UEs in a statistical sense.

## ✧ Interference modeling

When considering a more practical system, reasonable assumptions should be made on the weights of RIS, to model signal influence from both the serving and interfering base stations. For example, it could be assumed that the serving RIS weight matrix is the optimal phase configuration of any target user, and the interference RIS weight may be an identity matrix or a random phase matrix.

## ✧ Topology modeling

Based on the traditional passive reflection of RIS to signals, the topology modeling for RIS panel is very important in terms of system performance. Specifically, the topology modeling parameters of the RIS node may include location parameters, spatial characteristics, and RIS scale parameters.

(1) RIS position parameters: azimuth  $\theta$ , height  $h$ , distance  $r$ ;

(2) Scale and spatial characteristics of RIS: number of RIS elements, orientation and pitch angle.

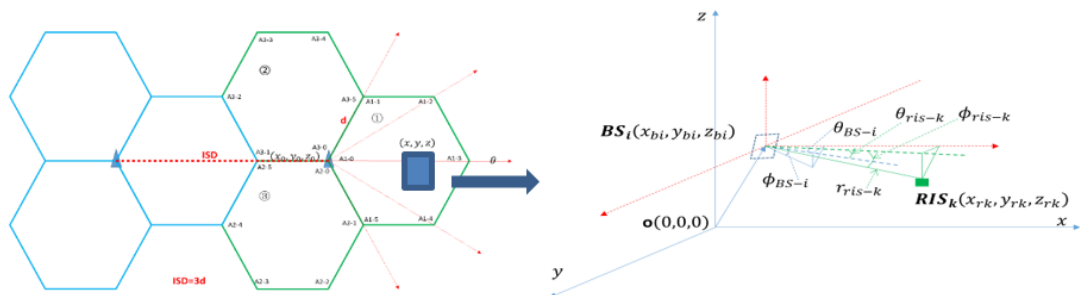


**Figure 3-8 RIS System Simulation Topology Modeling**

### 3.2.1.2. Simulation Parameters

The key parameters of the system level simulations are summarized in Table 3-2.

**Table 3-2 Parameters for system-level simulations**

System level simulation assumption	
Parameters	Values
Scenario	21/57 RRU, 10 UEs per RRU
Inter-Site Distance	300 m
Carrier Frequency/ Subcarrier Spacing	10 GHz/30GHz, 30 kHz
Simulation BW	20 MHz

Channel Model	BS-RIS,BS-UE UMa, RIS-UE UMi
UE Distribution	80% indoor, 20% outdoor, 3 km/h
RIS Panel Configuration	128/256/512/1024/2048
RIS Panel Number	1 RIS per sector

### 3.2.2. Simulation Results

#### 3.2.2.1. Impact of RIS topologies

This section analyzes UE Geometry performance with different assumptions on the RIS topology, panel scale, and assumptions of BS-RIS-UE or BS-UE channel. The results were analyzed at 10 GHz and 30 GHz frequencies respectively. Specifically, we consider four different RIS topologies at 10 GHz and consider different RIS scales at 30 GHz.

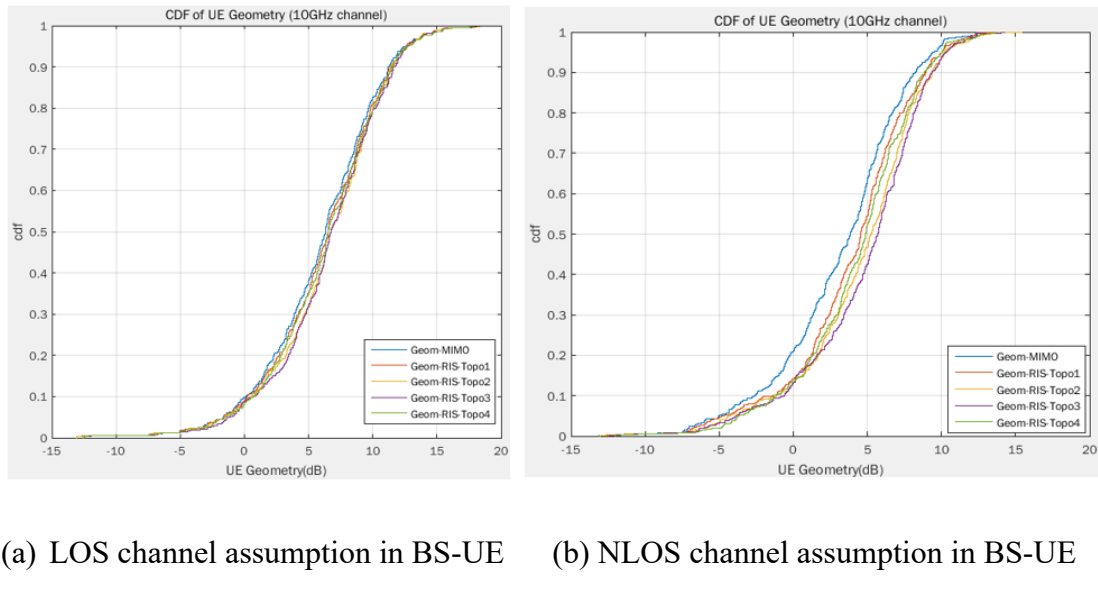
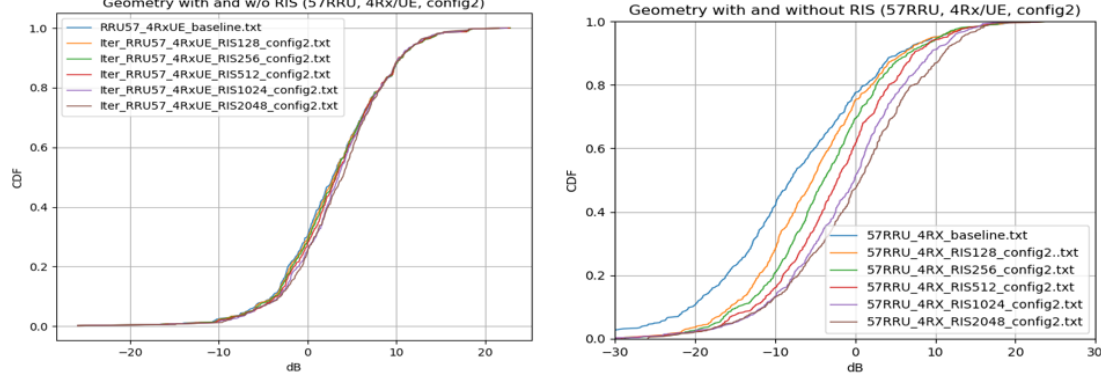


**Figure 3-9 Impact of RIS Topology on UE Throughput (10 GHz)**



(a) LOS assumption in BS-UE

(b) NLOS assumption in BS-UE

**Figure 3-10 Impact of RIS Topology on UE Throughput (30 GHz)**

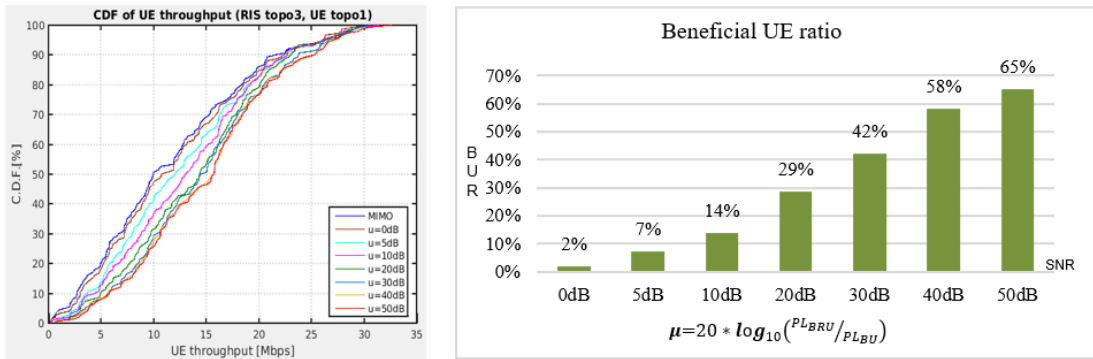
It is easy to find that the UE Geometry performance varies with the RIS topology, RIS scale, and BS-UEs and BS-RIS-UEs channel assumptions. Generally, when the direct channel is with relatively good quality, the Geometry gains are small regardless of the RIS topology and RIS scale. Only when the quality of the direct channel quality deteriorates, the performance gain of the RIS could be observed obviously.

### 3.2.2.2. Impact of RIS and UE distribution

The defined BUR greatly affects the performance space of the RIS system. In this section, the influence of BUR on UE throughput is analyzed.

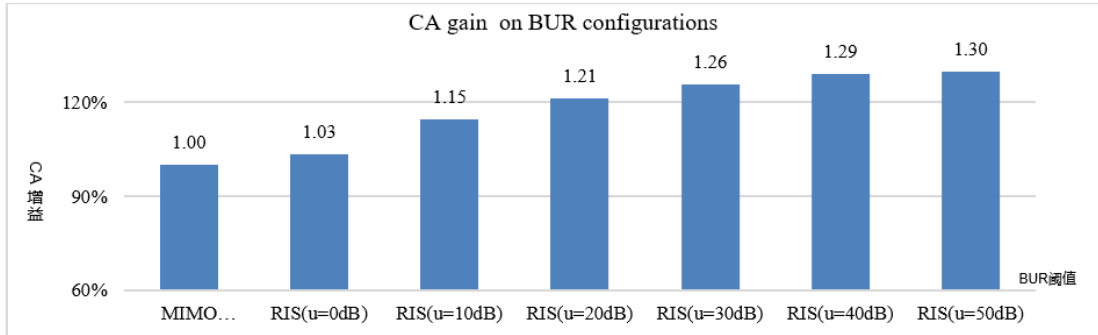
Specifically, to evaluate the BUR impact, 7 different levels of BUR thresholds are considered to reflect different benefit ratios and the corresponding performance gains.

As can be seen in **Figure 3-11**, user throughput performance increases as RIS BUR increases. When the proportion of benefited UEs accounts for 2% of the total number of UEs in the system, the gain of RIS compared with the baseline MIMO is only 3%. When the proportion of benefited UEs reaches 30%, RIS brings a large gain in user throughput, for example, a 20% increase in performance compared with the baseline MIMO.



(a) CDF of UE throughput

(b) BUR distribution with SNR assumptions



(c) Average cell throughput gains with different BUR thresholds

**Figure 3-11 User throughput performance**

Easy to find that in the simulations, BUR assumption is very important to identify the potential performance space of RIS system. Therefore, the gain of RIS system should be more objectively and fairly reflected with aligned BUR assumptions in the subsequent SLS performance evaluation and potential standardization process.

## 4. Conclusion

The increasing demands of future wireless networks highlight the need for more efficient and intelligent communication systems. Reconfigurable Intelligent Surfaces (RIS) have emerged as a promising solution, offering the potential to revolutionize wireless communication by manipulating electromagnetic wave propagation to create programmable wireless environments. Accurate channel modeling and simulation are essential for evaluating RIS performance and guiding the development of related technologies.

This white paper has provided a comprehensive overview of channel modeling and simulation for RIS, highlighting the latest research findings and offering insights for future research directions.

The RIS channel model builds upon 3GPP TR 38.901 by introducing a cascaded framework that jointly models the BS-RIS and RIS-UE sub-channels. Path loss is characterized by using modified FI (Floating Intercept) and CI (Close-In) models, which incorporate distance, angle dependencies, and RIS reflection gain, along with a Power Control Factor (PCF) to normalize cascaded and direct channel coupling. For fast fading, a GBSM-based cascaded model convolves multipath components from both sub-channels while maintaining spatial consistency and polarization effects, with complexity reduced through power-based cluster pruning. The RIS physical model employs RCS (Radar Cross Section) or approximations based on 3GPP TR 38.901 antenna patterns, accounting for near-field effects in large RIS panels. Key enhancements include updates to LOS probability, K-factor, delay/angle spread, and spatial consistency for dynamic environments, as well as discussions on reciprocity between TDD/FDD systems. This comprehensive framework enables accurate yet tractable RIS performance evaluation across diverse scenarios (UMi, UMa, InH), balancing realism with computational efficiency.

System-level simulations have shown the significant impact of RIS deployment strategies on network performance. Results indicate that deploying fewer, larger RIS panels (e.g.,  $40 \times 40$  elements) is more effective than deploying a larger number of smaller panels (e.g.,  $16 \times 16$  elements) in terms of SINR gains and coverage enhancement. Near-field propagation effects become more pronounced with larger RIS

panels, necessitating new designs for phase shifts and channel state information (CSI) feedback mechanisms. Additionally, the interference caused by RIS reflections has been shown to be minimal, especially for larger panels with narrow beams.

Topology optimization, including panel orientation and tilt toward serving base stations, is critical for maximizing cascaded link gains, with the Beneficial UE Ratio (BUR) metric effectively identifying optimal configurations. Practical constraints like 2-bit phase quantization and element spacing must balance performance and cost, though higher precision may benefit advanced beamforming. The results validate RIS as a coverage-enhancing solution, particularly for cell-edge users, with manageable interference and clear deployment trade-offs. These findings provide actionable insights for RIS integration in 5G-Advanced and 6G networks, though further research is needed for higher-frequency bands (e.g., 6.7 GHz) and ISAC integration. The study underscores RIS's potential while highlighting the importance of panel size, placement, and near-field adaptation for real-world implementation.

In conclusion, RIS technology holds great promises for enhancing wireless communication systems. The channel modeling and simulation work presented in this paper provides a solid foundation for further research and development. Future work should focus on refining the models to better capture the complexities of real-world deployments, exploring new optimization strategies for RIS configurations, and addressing the challenges posed by near-field effects and spatial consistency. As RIS continues to evolve, it is expected to play a key role in the development of 6G and beyond, contributing to the realization of highly efficient, low-latency, and wide-coverage wireless networks.

## Acronyms

<b>Abbreviation</b>	<b>Full Term</b>
RIS	Reconfigurable Intelligent Surface
3GPP	3rd Generation Partnership Project
ISAC	Integrated Sensing and Communication
UMi	Urban Micro
UMa	Urban Macro
InH	Indoor Hotspot
IIoT	Industrial Internet of Things
BS	Base Station
UE	User Equipment
PL	Path Loss
LOS	Line of Sight
PLE	Path Loss Exponent
SF	Shadow Fading
CI	Close-In
FI	Floating-Intercept
GBSM	Geometry-Based Stochastic Model
AoA	Angle of Arrival
AoD	Angle of Departure
ZoA	Zenith Angle of Arrival
ZoD	Zenith Angle of Departure
XPR	Cross-Polarization Power Ratio
DS	Delay Spread

ASA	Azimuth Spread of Arrival
ASD	Azimuth Spread of Departure
ZSA	Zenith Spread of Arrival
ZSD	Zenith Spread of Departure
TDD	Time Division Duplex
FDD	Frequency Division Duplex
RSRP	Reference Signal Received Power
SINR	Signal-to-Interference-plus-Noise Ratio
CSI	Channel State Information

## Reference

- [1] 3GPP, "Study on Channel Model for Frequencies from 0.5 to 100 GHz," Technical Specification (TR) 38.901, 3rd Generation Partnership Project (3GPP), 03 2022. Version 17.0.0.
- [2] H. Gong, *et al*, "How to Extend 3-D GBSM to RIS Cascade Channel With Non-Ideal Phase Modulation?," *IEEE Wireless Communications Letters*, vol. 13, no. 2, pp. 555-559, Feb. 2024.
- [3] J. Dou, *et al*. "On the channel modeling of intelligent controllable electro-magnetic-surface.", *Chinese journal of radio science*, 2021, 36(3): 368-377. (in Chinese)
- [4] W. Tang, *et al*, "Path Loss Modeling and Measurements for Reconfigurable Intelligent Surfaces in the Millimeter-Wave Frequency Band," *IEEE Trans. Commun.*, vol. 70, no. 9, pp. 6259-6276, Sept. 2022.
- [5] Y. Yuan, *et al*, "A Geometry-based RIS-assisted multi-user channel model with deep reinforcement learning," in *Proc. IEEE VTC-spring*, accept, 2024.
- [6] Y. Yuan, *et al*, "Characterization and modeling of RIS-assisted multi-user channels utilizing deep reinforcement learning," *IEEE Transactions on Communications*, under review, 2024.
- [7] Y. Yuan, *et al*, "RIS-assisted mobile channels with directional transmission: Modeling and characteristic analysis," *IEEE Transactions on Wireless Communications*, under review, 2024.
- [8] Y. Li, *et al*. "Path loss modeling for the RIS-assisted channel in a corridor scenario in mmwave bands," *2022 IEEE Globecom Workshops (GC Wkshps)*, Rio de Janeiro, Brazil, 2022, pp. 1478-1483.
- [9] J. Sang, *et al*., "Multi-scenario broadband channel measurement and modeling for sub-6 GHz RIS-assisted wireless communication systems," *IEEE Trans. Wireless Commun.*, vol. 23, no. 6, pp. 6312-6329, Jun. 2024.
- [10] J. Zhang, *et al*, "Cascaded channel modeling and experimental validation for ris assisted communication system," *2024 IEEE Globecom Workshops (GC Wkshps)*, 2024, accepted, yet to be presented.

- [11] J. Sang, *et al.*, “Measurement-Based Small-Scale Channel Model for Sub-6 GHz RIS-Assisted Communications,” *IEEE Trans. Veh. Technol.*, early access, 2024.
- [12] J. Sang, *et al.*, “Quantized Phase Alignment by Discrete Phase Shifts for Reconfigurable Intelligent Surface-Assisted Communication Systems,” *IEEE Trans. Veh. Technol.*, vol. 73, no. 4, pp. 5259-5275, Apr. 2024.
- [13] R1-2403285, Discussion on modeling near-field propagation and spatial non-stationarity in TR38.901 for 7-24GHz, 3GPP TSG RAN WG1 #116bis, April 15th – April 19th, 2024. (BUPT, CMCC)
- [14] R1-2404330, Discussion on modeling near-field propagation and spatial non-stationarity in TR38.901 for 7-24GHz, 3GPP TSG RAN WG1 #117, May 20th – 24th, 2024. (BUPT, CMCC, vivo)
- [15] R1-2406743, Discussion on near-field propagation and spatial non-stationarity, 3GPP TSG RAN WG1 #118, Aug 19th – Aug 23th, 2024. (BUPT, CMCC)
- [16] H. Miao, *et al.*, “Analysis of Near-Field Effects, Spatial Non-Stationary Characteristics Based on 11-15 GHz Channel Measurement in Indoor Scenario.” in IEEE Signal Processing Advances in Wireless Communications (SPAWC)., Sep. 2024.
- [17] Z. Yuan, *et al.*, "Spatial Non-Stationary Near-Field Channel Modeling and Validation for Massive MIMO Systems," in *IEEE Transactions on Antennas and Propagation*, vol. 71, no. 1, pp. 921-933, Jan. 2023
- [18] W. Tang, *et al.*, “On channel reciprocity in reconfigurable intelligent surface assisted wireless networks,” *IEEE Wireless Communications*, vol. 28, no. 6, pp. 94–101, Dec. 2021.
- [19] Q. Gu, D. Wu, X. Su, *et al.*, “System-level simulation of RIS assisted wireless communications system”. *GLOBECOM 2022 - 2022 IEEE global communications conference*, 1540–45, 2022.
- [20] Y. Yuan, Y. Huang, X. Su, *et al.*, Reconfigurable Intelligent Surface System Level Simulations for Industry Standards. *IEEE Communications Magazine*, 2025: 1-7.
- [21] W. Miao, J. Dou, *et al.*, “Physical modeling of reconfigurable intelligent surface for channel modeling,” *China Communications*, 2025, vol. 22, no. 2, pp. 128-142. DOI: 10.23919/JCC.fa.2023-0541.202502.
- [22]

